Published in final edited form as:

Mol Cell Neurosci. 2015 March ; 65: 143–152. doi:10.1016/j.mcn.2015.03.009.

Transcriptional Regulation of N-acetylaspartate Metabolism in the 5xFAD Model of Alzheimer's Disease: Evidence for Neuron-Glia Communication During Energetic Crisis

Samantha Zaroff[1,2], **Paola Leone**[1], **Scott W. J. McPhee**[3], **Vladimir Markov**[1], and **Jeremy S. Francis**[1,*]

[1]Cell & Gene Therapy Centre, Department of Cell Biology, Rowan University School of Osteopathic Medicine, Stratford, NJ USA

[2]Graduate School of Biomedical Sciences, Rowan University School of Osteopathic Medicine, Stratford, NJ USA

[3]Asklepios Biotherapeutics Inc., NC, USA

Abstract

N-acetylaspartate (NAA) provides a non-invasive clinical index of neuronal metabolic integrity across the entire neurodegenerative spectrum. While NAA function is not comprehensively defined, reductions in the brain are associated with compromised mitochondrial metabolism and are tightly linked to ATP. We have undertaken an analysis of abnormalities in NAA during early stage pathology in the 5xFAD mouse model of familial Alzheimer's disease and show here that dysregulated expression of the gene encoding for the rate-limiting NAA synthetic enzyme (Nat8L) is associated with deficits in mitochondrial oxidative phosphorylation in this model system. Downreguation of *Nat8L* is particularly pronounced in the 5xFAD hippocampus, and is preceded by a significant upregulation of oligodendrocytic *aspartoacylase* (*aspa*), which encodes for the sole known NAA-catabolising enzyme in the brain. Reductions in 5xFAD NAA and *Nat8L* cannot be accounted for by discrepancies in either neuron content or activity of the substrate-providing malate-aspartate shuttle, thereby implicating transcriptional regulation in a coordinated response to pathological energetic crisis. A central role for ASPA in this response is supported by a parallel developmental analysis showing highly significant increases in *Nat8L* expression in an ASPA-null mouse model during a period of early postnatal development normally punctuated by the transcriptional upregulation of *aspa*. These results provide preliminary evidence of a signaling mechanism in Alzheimer's disease that involves cross talk between neurons and oligodendrocytes, and suggest ASPA acts to negatively regulate *Nat8L* expression. This mechanism is proposed to be a fundamental means by which the brain conserves available substrate during energy crises.

*Corresponding author: 2 Medical Center Drive, SC253, Stratford, NJ, USA, Ph. 8565666050, francijs@rowan.edu.

Introduction

The brain is an energy-intensive organ that relies on an uninterrupted supply of substrate for mitochondrial oxidative phosphorylation to function. Processes such as the maintenance of action and synaptic potential contribute to a level of energy use that accounts for around 25% of the bodies total glucose budget (Attwell and Laughlin, 2001). The fundamental importance of glucose-derived energy for normal brain function (Magistretti, 2008) is reinforced by the prominence of markers of energetic crisis linked to compromised glucose metabolism in many neurodegenerative diseases. Neuronal metabolic integrity is inexorably linked to energetic stasis and, in this context, the abundant acetylated aspartate derivate N-acetylaspartate (NAA) is noteworthy. The readily detectable ^{1}H-MRS NAA signal provides a non-invasive index of neuronal metabolic integrity that is predictive for progression, recovery, and remission in an ever-increasing catalogue of disorders of the brain. The fundamental role of NAA in the brain remains enigmatic however, and experimental evidence for function has long been limited to a role in providing acetyl groups for lipid synthesis (D'Adamo et.al. 1968). This functional definition is of direct relevance to developmental myelination and places an emphasis on NAA catabolism by oligodendrocytic aspartoacylase (Chakraborty et.al. 2001; Madhavarao et.al. 2005), the sole known NAA-catabolizing enzyme in the brain. The importance of NAA catabolism by aspartoacylase (ASPA) to myelination is highlighted by the severely dysmyelinated phenotype of the inherited human pediatric leukodystrophy Canavan disease (CD), which results from the loss of ASPA function (Kaul et.al. 1991). Naturally, chronically elevated NAA is diagnostic for CD, but this association between pathology and abnormally high levels of NAA contrasts starkly with the abnormally low levels NAA characteristically seen in practically all other studied neurodegenerative contexts. The definition of NAA as solely a shuttle for acetyl groups during lipid synthesis is therefore incompatible with the general prominence of NAA as a prognostic marker of metabolic integrity across a broad pathological spectrum.

NAA is synthesized in neurons by the acetylation of mitochondrial-derived aspartate by an N-acetyltransferase that utilizes AcCoA drawn from the tricarboxylic acid (TCA) cycle, making NAA synthesis an energy-intensive process that is limited by available substrate from sources that are intimately coupled to ATP (Bates et.al. 1996). Because fluctuations in NAA closely parallel ATP during neuronal energetic crisis (Vagnozzi et.al. 2005), it is reasonable to hypothesize that such fluctuations are representative of a dynamic, coordinated response to energetic crisis that forms part of a key signaling mechanism with general relevance. Evidence in support of a mechanism of this nature has been recently generated in a model of traumatic brain injury (DiPetro et.al. 2014), and the present study was undertaken to explore the possibility of a comparable response in an *in vivo* model of familial Alzheimer's disease (AD).

Materials and Methods

Animals

5xFAD mice were maintained as a colony at the Rowan SOM animal facility established from founder animals obtained from the Mutant Mouse Regional Resource Center Network. The 5xFAD model has been described in detail elsewhere (Oakley et.al. 2006; https://

www.mmrrc.org/catalog/sds.php?mmrrc_id=34840). All procedures performed were done so under an approved Rowan-SOM IACUC protocol, and adhered to national and institutional guidelines for animal care and use. Animals were housed with ad libitum access to food and water. For all analyses detailed here, tissue was obtained post mortem from animals humanely euthanized with an intraperitoneal injection of sodium pentobarbital.

HPLC

5X FAD mice were deeply anesthetized and brains rapidly excised then flash frozen in liquid nitrogen. One intact hemisphere was used to prepare HPLC samples with 2× volume/weight of freshly prepared ice-cold precipitation solution (3:1 acetonitrile: KH_2PO_4 (pH 7.4). Tissue was homogenized with a dispersal element (Ultra Turrax, IKA Works Inc., NC, USA), and homogenates centrifuged for 10 minutes at 10,000×g at 4°C. The supernatant retained, and the remaining pellet sonicated with an additional 500µl of precipitation solution before centrifugation for 10 minutes at 10,000×g at 4°C. The two supernatants were combined and extracted twice with 2× volume of HPLC-grade chloroform. Samples were aliquoted and stored at -80°C until needed for HPLC analysis. Samples were run on a Thermo scientific Surveyor-Plus HPLC system equipped with UV detection and a Hypersil BDS-C18 column (5 µm particle size; 25× 4.9 mm). An ion-paired reverse phase detection methodology was used to analyze samples using buffers and sequence as described previously (Francis et.al. 2012). NAA, ATP, and AMP were quantified in a single run using standard curves generated by purified HPLC-grade standards. Quantities of each metabolite were expressed as a molar concentration per wet weight of tissue.

Quantitative Real Time RT-PCR

Total RNA was prepared from one entire hemisphere of flash frozen mouse brain (remaining from preparation of HPLC samples). Tissue was homogenized using Trizol reagent (Invitrogen Corp., Carlsbad, Ca) as per manufacturers instructions (1ml per 50-100mg tissue). Purified RNA was treated with DNase to remove contaminating genomic DNA and cleaned using RNeasy columns (Qiagen, Valencia, Ca). The concentration of all purified RNA was determined by spectophotometry and the integrity of samples verified by denaturing agarose/formaldehyde gel electrophoresis. cDNA for quantitative real-time RT-PCR (QRT-PCR) was generated from 1µg of purified RNA using a Superscript First Strand Synthesis Kit (Invitrogen, Carlsbad, CA). QRT-PCR was performed with Syber Green on an Applied Biosystems Step One Real Time PCR system (Applied Biosystems, Foster City, Ca). The primers for target transcripts were as follows: *Nat8L* (5′-3′; F: CTACCTGGAGTGCGCGCT, R: GGCGGCTTCATGTAGTACTGC), *ASPA* (5′-3′; F: TGAGCATCCTTCACTCAAATATGC, R: GGCTGAGGACCAACTTCTATACCA), and *NduSF2* (5′-3′; F: AGGTTGATGACGCCAAAGTGT, R: GACTCCATGGACGTCTTCATCTC). The Relative Standard curve method was used to analyze *Nat8L*, and the ΔCT method used for *ASPA* and *NduSF2* after validating primer efficiency with a *GAPDH* internal reference.

In Situ Hybridization

Nat8L mRNA was visualized in intact tissue using a digoxigenin-UTP labeled RNA probe (DIG-Nat8L) synthesized from the first 830bp of the mouse *Nat8L* CDS. The 830bp *Nat8l* region was amplified from 4-week old mouse brain mRNA by RT-PCR and subcloned into a TOPO-TA plasmid for sequencing. The *Nat8L* CDS was then subcloned into the plasmid pSPT-19 for synthesis of DIG-Nat8L using a commercially available kit, following the manufacturers instructions (Roche Diagnostics, IN, USA). DIG-Nat8L was hybridized with 45μm free floating coronal sections at a concentration of 30 ng/ml for 20 hours at 55°C. After hybridization, sections were washed and blocked and incubated for 2 hours with anti-DIG-AP antibody at a dilution of 1:20,000. For co-labeling with NeuN, DIG-Nat8L labeled sections were then incubated overnight in NeuN (1:5000) prior to mounting and coverslipping.

Immunohistochemistry

All tissue samples for immunohistochemistry were prepared by the transcardial perfusion of deeply anesthetized animals with ice cold 0.9% saline followed by freshly prepared 4% buffered paraformaldehyde. Perfused brains were removed and post-fixed overnight in 4% paraformaldehyde, then cryopreserved in an ascending sucrose gradient. Cryopreserved brains were embedded in Tissue-Tek OCT compound (Sakura, Torrance, Ca), and flash frozen in an Isopentane/dry ice bath. Serial 45 um sections were collected from each brain (beginning approximately from Bregma 0.20mm) and stored at -20°C in cryoprotectant until needed. Free-floating sections were incubated in primary antibodies overnight at room temperature (RT) in immunobuffer (1× PBS, 0.1% Triton X-100, and 1% normal goat serum; mouse A60 neuron-specific nuclear protein [NeuN] 1:500 [Millipore, Billerica, Ma], mouse aspartoacylase (ASPA) 1:250 [Francis et.al. 2007]). After incubation in primary antibody, sections were incubated for 2 hours at RT in biotinylated secondary antibody (Sigma-Aldrich, St. Louis, Mo), followed by incubation at RT for 1 hour in extravadin peroxidase (Sigma-Aldrich, St. Louis, Mo). Positive cells were visualized using 3, 3′-diaminobenzidine (DAB). Developed sections were mounted onto glass slides, dehydrated in an ascending ethanol gradient, and then cleaned twice with xylene and coverslipped with DPX mountant (Sigma-Aldrich, St. Louis, Mo).

Unbisaed Stereology

Estimates of NeuN-positive neurons were generated using the optical fractionator (k=4) and Stereologer software (Stereology Resource Center, Tampa, FL). Counts were performed on a single hemisphere of processed sections to generate estimates of NeuN for CA1 of the hippocampus and cortical layer V for 5xFAD and age matched control brains, and the thalamus and the stratum radiatum of the hippocampus of 2-week *nur7* and age matched control brains. All counts were performed at the 100× objective on an Olympus BX51 upright microscope equipped with an analogue camera and motorized stage. Significance differences in *N* between experimental and control groups were determined by a 2-tailed students T-test ($p \leq 0.05$).

Microarray Analysis of Mitochondrial Gene Expression

The expression of 84 nuclear encoded transcripts for components of the mitochondrial electron transport chain (Complexes I-V) was analyzed using commercially available RT^2 Profiler™ Mouse Mitochondrial Arrays (SA Biosciences/Qiagen). Total RNA was isolated from one hemisphere of flash frozen brains with Trizol reagent as described. 0.5μg of purified RNA from 4-month WT and 4- month 5X FAD brains was used to prepare cDNA using the RT^2 First Strand Synthesis Kit, as per the manufacturers instructions. The resulting cDNA was combined with RT^2 Syber Green Master mix and added to the wells of a mouse mitochondrial energy metabolism RT^2 Profiler PCR array. The prepared plate was run on an Eppendorf Mastercycler Ep Realplex 4S. The fold change of each target gene in 5X FAD samples relative to wild type controls was determined using the CT to fold change RT^2 Profiler PCR Array Data Analysis Template V4.0. Significant differences in 5xFAD expression were determined using a threshold significance of $p<0.005$.

Mitochondria Isolation, Complex I Assay, and Malate Aspartate Shuttle Assay

Intact mitochondria were isolated from flash frozen brain tissue. Tissue was homogenized in 6ml of homogenization buffer (320 mM Sucrose, 10 mM Tris-HCL [pH 7.4], 2 mM EDTA), and centrifuged for 10 minutes at 1000×g to pellet cell membranes and debris. The supernatant was removed and centrifuged for 20 minutes at 20,000×g to pellet mitochondria. The mitochondrial pellet was re-suspended in 1ml of homogenization buffer without EDTA, and total protein concentration determined by BCA Protein Assay Kit (Thermo Fischer Scientific, Rockford, Il).

Malate aspartate shuttle (MAS) activity in intact mitochondria isolated from brains was assayed using previously published methodology (Jalil et al, 2006). Briefly, mitochondria (100mg/sample) were placed in triplicate into a 96 well plate, and assay solution containing assay buffer (75 mM mannitol, 20 mM Tris-HCl, 0.5 mM EDTA, 100mM KCL, 5 mM phosphate, 0.1% BSA) and reaction solution (66.6 mM NADH, 5 mM aspartate, 5 mM malate, 0.5 mM ADP, 16 mM CaCl2, and 5 mM glutamate) added. The reaction was started by the addition of 4U/ml aspartate aminotransferase and 6U/ml of malate dehydrogenase to each well. Shuttle activity was defined by the oxidation of NADH over 5 minutes as determined by the change in OD at 340nm on an automated microplate reader (BioTek Instruments Inc. Winooski, VT).

Mitochondrial complex I activity was determined for the same intact mitochondrial samples using a commercially available immunocapture microplate format kit (abcam, Cambridge, Ma). Briefly, mitochondrial proteins were generated by detergent extraction of intact samples followed by centrifugation. Lysed samples were then diluted to 250 ug/ml with supplied buffer, and 200μl added in triplicate to the microplate supplied with the kit. Samples were incubated at room temperature for 3 hours, washed, and 200 ul of assay solution (1× Buffer, 1× NADH, and 1× dye) added. The absorbance of wells was read at 450nm every minute for 30 minutes using a Microplate reader (BioTek, Winooski, VT). Complex I activity was expressed as the average change in absorbance/min/ug of total protein over 30 minutes.

Results

Significant Reductions in NAA involve a downregulation of Nat8L Expression in the 5xFAD mouse Brain

Reductions in NAA are a feature of early pathology in animal models of AD (Lalande et.al. 2014; Dedeoglu et.al. 2004) and in affected humans (Godbolt et.al. 2006). The 5xFAD mouse, which harbors five familial AD mutations, presents with the accumulation of soluble and insoluble Aβ42 from 2 months of age, cortical and hippocampal cell loss from 6 months of age, and progressive cognitive decline from 6 months of age (Oakley et.al. 2006). Homogenates of whole brain 5xFAD tissue were analyzed for NAA by HPLC at 1, 2, and 4 months of age to identify reductions at early stages pathology prior to detectable neuronal loss (Fig.1). 1-month old 5xFAD brains showed no differences in whole brain NAA relative to wild type controls, while 2-month 5xFAD brains presented with a small reduction in NAA that did not approach statistical significance. 4-month 5xFAD brains showed a statistically significant decrease in NAA relative to wild type controls, suggesting the downregulation of NAA synthesis from 2-4 months of age (Fig.1A). The gene encoding for the rate-limiting NAA synthetic enzyme N-acetyltransferase 8-like has been identified (*Nat8L*; Wiame et.al. 2009), and recently published studies have documented reduced expression of *Nat8L* in association with a pathological lowering of whole brain NAA (DiPietro et.al. 2014). In order to assess the possibility of a similarly coordinated effect on 5xFAD NAA metabolism, QRT-PCR for *Nat8L* was performed on whole brains at 2 and 4 months of age (Fig.1B). While a trend for decreased *Nat8L* expression at 2 months of age in 5xFAD brains was not statistically significant (p=0.14), 4-month old 5xFAD brains manifest a highly significant 2.5-fold decrease in expression (p=0.0094). *In situ* patterns of *Nat8L* expression in 4-month 5xFAD brains were assessed using a digoxigenin -labelled RNA probe, revealing a prominent decrease in the CA1 subfield of the hippocampus (Fig.1C), an area of anatomy of relevance to well-documented spatial learning deficits in this model system.

5xFAD mice suffer from cell loss in cortical layer V from 6 months of age onwards (Eimer and Vasser, 2013), and differences in neuron content would be expected to contribute to reductions in both NAA and *Nat8L*. *Nat8L*-positive cells co-labeled with neuronal nuclear antigen (NeuN) in the present study (Fig.2A&B) and in order to normalize for relative neuron content, stereological estimates for cortical layer V and hippocampal CA1 NeuN-positive cells were generated for 4-month 5xFAD and wild type brains. Numbers of NeuN-positive cells in both cortical layer V (Fig.2C) and hippocampal CA1 (Fig.2D) were not significantly different from wild type controls at 4-months (p=0.331, and p=0.741, respectively), ruling out cell loss as a cause of observed reductions in NAA and *Nat8L*.

Reductions in NAA coincide with impaired mitochondrial function

Pathological changes in NAA have a well-documented association with cellular energetic status (Vagnozzi et.al. 2005) that suggests reductions occur in response to depleted energetic resources. 2 and 4-month 5xFAD brains were analyzed for ATP and AMP levels by HPLC to explore the possibility of a temporal relationship between abnormalities in these connected metabolic indices (Fig.3). ATP was significantly reduced at both 2 and 4-months

of age in 5xFAD mice (Fig.3A), with 2-month reductions being of greater significance. AMP was increased significantly in 2-month 5xFAD brains, but not in 4-month brains (Fig3B), while the ATP/AMP ratio was significantly lower at both ages in 5xFAD brains (Fig.3C), again, with the 2-month reduction being more significant than the 4-month reduction, suggesting changes in NAA and *Nat8L* are preceded by a loss of energetic integrity.

NAA synthesis is coupled to mitochondrial oxidative phosphorylation in neurons (Bates et.al. 1996) and compromised mitochondrial function in 5xFAD brains would be expected to impact negatively on NAA. However, how mitochondrial function might impact *Nat8L* expression is less clear-cut, but an active downregulation in oxidative phosphorylation may be a marker of a regulatory stimulus linking NAA to reductions in the ATP/AMP ratio. 4-month old 5xFAD brains were analyzed for the expression of 84 nuclear encoded components of the electron transport chain by microarray to assess the overall status of oxidative phosphorylation. Using a threshold significance value of $p \leq 0.005$, a total of 13 genes were identified as significantly downregulated in 5xFAD brains, five representing Complex I, none representing Complex II, three representing Complex III, two representing Complex IV, and three representing Complex V (Table 1). In-house QRT-PCR was used to validate array data for the most significantly downregulated Complex I gene, *Ndusf2* at 4 months, and to determine possible representative differences at 2 months of age (Fig.4A). A highly significant downregulation of *Ndusf2* in 4-month old 5xFAD brains was confirmed, with no significant difference in expression evident at 2 months. Importantly, this 4-month reduction in *Ndusf2* was not due to differences in mitochondrial genome copy number, as determined by QPCR (5xFAD *Cox2* copy number fold-wild type *Cox2* copy number = 1.212, $p=0.8$; $n=4$), indicating a general downregulation of mitochondrial function in the absence of a reduction in mitochondria content at 4-months of age in 5xFAD brains. Consistent with the downregulation mitochondrial function inferred by the reduced expression of genes encoding components of the electron transport chain, isolated intact mitochondria prepared from 5xFAD brains presented with a significant decrease in Complex I activity at 4-months, while a smaller decrease in activity at 2-months did not achieve statistical significance (Fig. 4B).

The coupling of NAA synthesis to mitochondria has a basis in a dependence on mitochondrial aspartate supplied via the malate-aspartate shuttle (MAS) (Jalil et.al. 2005). It is conceivable, therefore, that reductions in 5xFAD whole brain NAA (Fig.1A) could be due to abnormally low MAS activity as much as to reduced *Nat8L* expression (Fig.1B). To clarify the relative contribution of MAS to NAA levels, intact mitochondrial fractions from 4-month brains were assayed for MAS activity (Fig.5). In contrast to observed reductions in Complex I activity (Fig.4B), MAS activity was significantly increased in 4-month old 5xFAD brains, making it unlikely that reductions in whole brain NAA can be accounted for by a decreased availability of rate-limiting aspartate.

Downregulation of Nat8L in 5xFAD Mice is preceded by increased ASPA expression

Currently, the only context in which experimental evidence for NAA function in the brain exists is developmental myelination, during which NAA acts as a carrier of acetyl groups for

fatty acid synthesis. This function requires the catabolic activity of the oligodendrocytic enzyme ASPA, reflecting a significant degree of cross talk between the neuronal and glial compartments. Early pathology in models of myelination lacking ASPA is punctuated by oxidative stress and energetic crisis (Francis et.al. 2012), which may provide a conduit through which pathological abnormalities in NAA in white matter and grey matter diseases can be linked. Because *aspa* expression during development is responsive to neuronal cues (Francis et.al. 2011), it is possible that reduced *Nat8L* expression in 5xFAD brains is part of a broader response to energetic crisis that is associated with concurrent abnormalities in the catabolic half of the NAA metabolic cycle. Indeed, recent evidence of dysregulated *aspa* expression in traumatic brain injury supports such a possibility (DiPietro et.al. 2014) and in order to explore this possibility in the 5xFAD system, 2 and 4-month brains were analyzed for *aspa* by QRT-PCR (Fig.6). 2-month 5xFAD brains manifest a significant increase in *aspa*, while 4-month 5xFAD brains presented with levels of *aspa* expression not significantly different from wild type controls (Fig. 6A), placing abnormalities in *aspa* downstream of abnormalities in *Nat8L*. ASPA immunohistochemistry in 2-month brains revealed increases in protein within white matter-rich areas of the internal capsule adjacent the thalamus (Fig.6B&C), subcortical white matter tracts of the external capsule overlying the hippocampus (Fig.6D&E), and white matter of the fornix of the hippocampus (Fig. 6F&G). Thus, downregulated neuronal *Nat8L* is preceded by an increase in *aspa* within white matter tracts, thereby implicating oligodendrocytes in the regulation of *Nat8L*.

Aspa expression is upregulated between 1-4 weeks of age during normal development (Kirmani et.al. 2003; Francis et.al. 2011). In order to identify a possible signaling hierarchy between *aspa* and *Nat8L*, *Nat8L* expression was analyzed by QRT-PCR in ASPA-null *nur7* mice (Traka et.al. 2008) at 1, 2 and 4 weeks of age (Fig.7). At 1 and, particularly, 2 weeks of age, *nur7* brains manifest a highly significant increase in *Nat8L* expression relative to wild type controls. *In situ* hybridization for *Nat8L* RNA in 2-week *nur7* brains revealed clear increases within the thalamus and interneurons of the hippocampus (Fig.7B-I), indicating a significant degree of transcriptional dysregulation within neuron-rich regions of the brain resulting from the loss of ASPA. Stereological estimates of NeuN-positive neurons with both the thalamus and the region of the hippocampus internal to CA1 and the dentate gyrus (area of increased *Nat8L* RNA [Fig. 7G]) of 2-week *nur7* brains reveled no significant differences in neuron content relative to wild type controls (Fig.7J&K), indicating differences in *Nat8L* expression are not due to abnormally high numbers of neurons in *nur7* brains, thus placing ASPA upstream of *Nat8L* in a signaling mechanism responsive to energetic crisis (Francis et.al. 2012).

Discussion

A consistent feature of pathological reductions in NAA in the brain is a tight association with energetic integrity. The energy-dependent nature of NAA synthesis is consistent with this association, and pathological reductions in NAA closely mimic changes in ATP (Signoretti et.al. 2001), suggesting a dynamic relationship between NAA synthesis and mitochondrial oxidative metabolism. Reductions in NAA can however occur by a number of distinct means, not all of which support the action of a targeted signaling mechanism. Firstly, cell death associated with disease or insult can reduce the synthetic capacity of the

neuronal compartment by way of a reduction in cell number. Secondly, limitations of substrate availability (Jalil et.al. 2005) or mitochondrial respiration (Bates et.al. 1996) will constrain the capacity of available neurons to maintain high levels of NAA synthesis independently of cell density (Vielhaber et.al. 2003). Thirdly, increased NAA catabolism by oligodendrocytic ASPA will result in a decrease in substrate independently of neuron loss or restricting mitochondrial function, as is the case with myelination during normal development following an increase in *aspa* expression (Kirmani et.al. 2004). Finally, NAA synthesis may be influenced via transcriptional regulation of the gene encoding for its synthetic enzyme, *Nat8L* (Wiame et.al. 2009) and, in terms of a dynamic interaction between NAA and energetic metabolism, is of particular interest. The present study shows the transcriptional downregulation of *Nat8L* in the 5xFAD mouse model of familial AD (Fig.1) in association with energetic crisis (Fig.3) and a reduction in mitochondrial oxidative phosphorylation (Fig.4). Importantly, reductions in all of these indices were manifest in the absence of detectable neuron loss (Fig.2), indicating a coordinated reduction in NAA synthesis in response compromised mitochondrial function. These observations build upon a considerable body of experimental data highlighting the tight coupling of NAA to available energy (Vagnozzi et.al. 2005), and place abnormalities in NAA at a very early stage of pathology in a model of a major neurodegenerative disease. Given that clinical reductions in NAA are invariably associated with disease progression in the brain, the elucidation of signaling mechanisms targeting the transcriptional regulation of components of NAA metabolism has potential relevance to the definition of diagnostic markers of the early stages of neurodegenerative disease. With respect to AD specifically, pathology is associated with a host of metabolic abnormalities that include oxidative stress (Nunomura et.al. 2006), mitochondrial dysfunction (Perry et.al. 1980; Gibson et.al. 1988) and deficits in glucose metabolism (Friedland et.al. 1983). Likewise, animal models of AD consistently manifest metabolic abnormalities (Nicholson et.al. 2010), more often than not prior to significant cognitive dysfunction (Chen et.al. 2012), with NAA constituting a widely cited metric of the integrity of these metabolic processes. The reason for the prominence of NAA in this context is not currently clear, but all of these metabolic indices represent potential regulatory stimuli.

NAA is not toxic (Karaman et.al. 2011), making it unlikely that the transcriptional downregulation of *Nat8L* presented here, and elsewhere (DiPietro et.al. 2014), results from a direct activation of signaling pathways by NAA itself. Instead, pathological reductions in NAA synthesis are more likely a component of a response to energetic crisis specifically. The significant upregulation of *aspa* immediately prior to reduced *Nat8L* in the 5xFAD brain (Fig.6) indicates this response is multicompartmental in nature and invites a definition of NAA function that is applicable to a broad neurodegenerative spectrum of relevance to both grey and white matter. A degree of metabolic reciprocity between these two compartments is requisite for such a definition, and the highly significant increase in *Nat8L* expression in the *nur7* mouse (Fig.7), which lacks ASPA, provides preliminary experimental evidence of the existence of this. Again, NAA does not directly activate signal transduction in oligodendrocytes (Kolodziejczyk et.al. 2009), suggesting ASPA links a regulatory hierarchy that begins with energetic deficit and culminates in the downregulation of *Nat8L*. ASPA currently features prominently in developmental myelination only, with expression

(Kirmani et.al. 2004) and activity (Bhakoo et.al. 2001) significantly upregulated after approximately 7 days of age in rodents. Transcriptional upregulation is independent of differences in oligodendrocyte number and is responsive to neuronal cues (Francis et.al. 2011), thereby providing a developmental example of regulatory reciprocity. In the present study, increased *aspa* in the 2-month 5xFAD brain was associated with a sharp decrease in the ATP/AMP ratio (Fig.3C), implicating ASPA in an initial response to energetic stress in a model of neurodegenerative disease. While this postulate appears inconsistent with the documented role of ASPA role in myelination, recent characterization of early pathology in a mouse model of CD reveals some informative associations of relevance to the present study. The *nur7* mouse is a model of CD that lacks detectable ASPA and presents with chronically elevated NAA, spongiform degeneration, and oligodendrocyte loss (Traka et.al. 2008). Gross pathology in the *nur7* brain is not readily apparent until 3-4 weeks of age, and prior to 2 weeks, myelin and oligodendrocyte content are unremarkable relative to wild type controls. We recently undertook an analysis of *nur7* pathology from 1-4 weeks of age from the perspective of the energetic demands of myelination, which revealed markers of oxidative stress at 2 weeks of age, prior to significant cell loss or dysmyelination (Francis et.al. 2012). These markers include reduced ATP, suggesting the onset of myelination in the absence of ASPA places increased demands on oxidative metabolism in the *nur7* brain. In the present study, *Nat8L* expression during this period of *nur7* development was significantly upregulated (Fig.7A), suggesting of a loss of feedback to neurons from oligodendrocytes subject to oxidative stress. It is not until 4 weeks of age, at the conclusion of the bulk of developmental myelination, that *Nat8L* expression normally increases (Fig. 7A), with 4 weeks in the *nur7* brain marking the onset of progressive cell loss, dysmyelination, and spongiform degeneration (Francis et.al. 2012). This order of events places transcriptional abnormalities in *Nat8L* (Fig.7) upstream of gross *nur7* pathology, but coincident with oxidative stress and ATP deficit, thereby drawing comparisons to energetic stress and downregulated *Nat8L* in the 5xFAD brain. The *nur7* energetic deficit likely occurs due to the diversion of AcCoA from energy generating reactions as a result of a dramatic reduction in available acetyl groups normally provided by the catabolism of NAA by ASPA. Postnatal myelination requires a significant physiological investment by oligodendrocytes that can see membranes grow as much as $5mm^2$/day (Pfieffer et.al. 1993) and consumes an estimated 3.33×10^{23} molecules of ATP per gram of tissue (Harris & Attwell, 2012). Viewed in these terms, myelination qualifies as a metabolic stress, with ASPA acting to alleviate energetic demand by the provision of substrate for a competing process, and the function of NAA as a shuttle for acetyl groups during lipid synthesis is not incompatible with the prominence of NAA as a maker of metabolic integrity. Based on the results of the present study, ASPA may also regulate energy-intensive NAA synthesis in neurons during myelination via the repression of *Nat8L* expression, thereby preventing a further dilution of energetic resources (AcCoA and aspartate) during myelination. The disinhibition of *Nat8L* of in the absence of ASPA and the downregulation of *Nat8L* following the activation of *aspa* supports the notion of high levels of NAA synthesis being detrimental to energetic integrity during both energy-intensive myelination and pathological energetic stress. NAA metabolism in both contexts is therefore linked by energetic integrity, arguing for a role more weighted towards the maintenance of overall metabolic homeostasis than to lipid synthesis. The argument becomes more compelling when the abundance of

NAA in the brain is considered. NAA is found in concentrations up to 10mM in whole brain, and within neurons this concentration approaches 20mM (Miller, 1991). The commitment of the requisite AcCoA and aspartate to maintain this level of NAA is a significant investment by neurons (Fig.8), and it is difficult to justify this investment in terms of lipid synthesis alone outside of developmental myelination, particularly when it competes with mitochondrial shuttling mechanisms for substrate (Ramos et.al. 2011). Indeed, reductions in 5xFAD NAA in the present study occurred in the face of reduced ATP (Fig.3A) and significant *increases* in MAS activity (Fig.5) suggestive of an effort to uncouple energy-intensive NAA synthesis from the provision of reducing equivalents for energy synthesis. Compromised mitiochondrial oxidative phosphorylation results in reduced pyruvate oxidation and entry into the TCA cycle. The NADH generated by cytosolic glycolysis will catalyze the conversion of pyruvate to lactate, resulting in a loss of available NADH. The MAS prevents the loss of NADH by shuttling reducing equivalent, in the form of malate, into mitochondria where it contributes to ATP synthesis. Thus, the MAS compensates for compromised mitochondrial respiration to a degree by providing NADH generated by glycolysis. High levels of NAA synthesis are incompatible with the compensatory function of the MAS due to a common requirement for aspartate. Thus, by not actively reducing NAA synthesis during energetic stress, the neuron risks compounding pathological reductions in ATP. Exactly how ASPA is able to affect such a mechanism in neurons is currently unknown, and beyond the scope of data presented here, but the repertoire of oligodendrocyte function is fast extending boundaries defined by myelination to include possible roles in the provision of energetic substrate to neurons (Morrison et.al. 2013; Saab et.al. 2013). NAA metabolic equilibrium is the product of an equilibrium struck between the synthetic and metabolic compartments. The primary determinants of the maintenance of this equilibrium are unknown, but the data presented here suggest input from a specific cellular compartment constitutes a signal for response by the corresponding compartment. Thus, the loss of ASPA function in oligodendrocytes appears to result in the dysregulation of *Nat8L* in neurons (Fig.7). Identification of primary determinants will likely require an analysis, complementary to the current study, of the regulation of both Nat8L and ASPA within the context of lipid synthesis and myelination in order to highlight common mechanisms. Evidence of the existence of signal transduction pathways that converge on NAA is not without precedent (Hirrlinger and Nave, 2014; DiPietro et.al. 2014), and should prompt a reassessment of the role of the complete NAA metabolic cycle in the brain with a view to defining function in the context of mechanisms that are relevant to the prominence of NAA in both disease and development.

Acknowledgments

This study was funded by an NIH/NIA STTR grant (Grant # 1R41G044890-01A1), the Boye Foundation Inc. (NJ), Canavan Research (IL), and the Silver Foundation (IL).

References

Attwell D, Laughlin SB. An energy budget for signaling in the grey matter of the brain. J Cereb Blood Flow Metab. 2001; 21:1133–1145. [PubMed: 11598490]

Bates TE, Strangward M, Keelan J, Davey GP, Munro PM, Clark JB. Inhibition of N-acetylaspartate production: implications for 1H MRS studies in vivo. Neuroreport. 1996; 7:1397–1400. [PubMed: 8856684]

Bhakoo KK, Craig TJ, Styles P. Developmental and regional distribution of aspartoacylase in rat brain tissue. J Neurochem. 2001; 79:211–220. [PubMed: 11595773]

Chakraborty G, Mekala P, Yahya D, Wu G, Ledeen RW. Intraneuronal N-acetylaspartate supplies acetyl groups for myelin lipid synthesis: evidence for myelin-associated aspartoacylase. J Neurochem. 2001; 78:736–745. [PubMed: 11520894]

Chen SQ, Cai Q, Shen YY, Wang PJ, Teng GJ, Zhang W, Zang FC. Age-related changes in brain metabolites and cognitive function in APP/PS1 transgenic mice. Behav Brain Res. 2012; 235:1–6. [PubMed: 22828014]

D'Adamo AF Jr, Gidez LI, Yatsu FM. Acetyl transport mechanisms. Involvement of N-acetyl aspartic acid in de novo fatty acid biosynthesis in the developing rat brain. Exp Brain Res. 1968; 5:267–273. [PubMed: 5712694]

Dedeoglu A, Choi JK, Cormier K, Kowall NW, Jenkins BG. Magnetic resonance spectroscopic analysis of Alzheimer's disease mouse brain that express mutant human APP shows altered neurochemical profile. Brain Res. 2004; 1012:60–65. [PubMed: 15158161]

Di Pietro V, Amorini AM, Tavazzi B, Vagnozzi R, Logan A, Lazzarino G, Signoretti S, Lazzarino G, Belli A. The molecular mechanisms affecting N-acetylaspartate homeostasis following experimental graded traumatic brain injury. Mol Med. 2014; 20:147–157. [PubMed: 24515258]

Eimer WA, Vassar R. Neuron loss in the 5XFAD mouse model of Alzheimer's disease correlates with intraneuronal A β42 accumulation and Caspase-3 activation. Mol Neurodegener. 2013; 8:2.10.1186/1750-1326-8-2 [PubMed: 23316765]

Friedland RP, Budinger TF, Ganz E, Yano Y, Mathis CA, Koss B, Ober BA, Huesman RH, Derenzo SE. Regional cerebral metabolic alterations in dementia of the Alzheimer type: positron emission tomography with [18F]fluorodeoxyglucose. J Comput Assist Tomogr. 1983; 7:590–598. [PubMed: 6602819]

Francis JS, Strande L, Pu A, Leone P. Endogenous aspartoacylase expression is responsive to glutamatergic activity in vitro and in vivo. Glia. 2011; 59:1435–1446. [PubMed: 21608034]

Francis JS, Strande L, Markov V, Leone P. Aspartoacylase supports oxidative energy metabolism during myelination. J Cereb Blood Flow Metab. 2012; 32:1725–1736. [PubMed: 22617649]

Gibson GE, Sheu KF, Blass JP, Baker A, Carlson KC, Harding B, Perrino P. Reduced activities of thiamine-dependent enzymes in the brains and peripheral tissues of patients with Alzheimer's disease. Arch Neuol. 1988; 45:836–840.

Godbolt AK, Waldman AD, MacManus DG, Schott JM, Frost C, Cipolotti L, Fox NC, Rossor MN. MRS shows abnormalities before symptoms in familial Alzheimer disease. Neurology. 2004; 66:718–722. [PubMed: 16534109]

Harris JJ, Attwell D. The energetics of central nervous system white matter. J Neurosci. 2012; 32:356–371. [PubMed: 22219296]

Hirrlinger J, Nave KA. Adapting brain metabolism to myelination and long-range signal transduction. Glia. 2014; 62:1749–1761. [PubMed: 25130164]

Jalil MA, Begum L, Contreras L, Pardo B, Iijima M, Li MX, Ramos M, Marmol P, Horiuchi M, Shimotsu K, Nakagawa S, Okubo A, Sameshima M, Isashiki Y, Del Arco A, Kobayashi K, Satrústegui J, Saheki T. Reduced N-acetylaspartate levels in mice lacking aralar, a brain- and muscle-type mitochondrial aspartate-glutamate carrier. J Biol Chem. 2005; 280:31333–31339. [PubMed: 15987682]

Karaman S, Barnett J Jr, Sykes GP, Hong B, Delaney B. Two-generation reproductive and developmental toxicity assessment of dietary N-acetyl-L-aspartic acid in rats. Food Chem Toxicol. 2011; 49:3192–3205. [PubMed: 21920405]

Kaul R, Gao GP, Balamurugan K, Matalon R. Cloning of the human aspartoacylase cDNA and a common missense mutation in Canavan disease. Nat Genet. 1993; 5:118–123. [PubMed: 8252036]

Kirmani BF, Jacobowitz DM, Namboodiri MA. Developmental increase of aspartoacylase in oligodendrocytes parallels CNS myelination. Brain Res Dev Brain Res. 2004; 140:105–115.

Kolodziejczyk K, Hamilton NB, Wade A, Káradóttir R, Attwell D. The effect of N-acetyl-aspartyl-glutamate and N-acetyl-aspartate on white matter oligodendrocytes. Brain. 2009; 132:1496–1508. [PubMed: 19383832]

Lalande J, Halley H, Balayssac S, Gilard V, Déjean S, Martino R, Francés B, Lassalle JM, Malet-Martino M. 1H NMR metabolomic signatures in five brain regions of the AβPPswe Tg2576 mouse model of Alzheimer's disease at four ages. J Alazheimers Dis. 2014; 39:121–143.

Madhavarao CN, Arun P, Moffett JR, Szucs S, Surendran S, Matalon R, Garbern J, Hristova D, Johnson A, Jiang W, Namboodiri MA. Defective N-acetylaspartate catabolism reduces brain acetate levels and myelin lipid synthesis in Canavan's disease. Proc Natl Acad Sci. 2005; 102:5221–5226. [PubMed: 15784740]

Magistretti, PJ. Brain Eenergy Metabolism. In: Squire; Berg; Bloom; du Lac; Ghosh; Spitzer, editors. Fundamental Neuroscience. San Diego: Academic Press; 2008. p. 271-293.

McKenna MC, Waagepetersen HS, Schousboe A, Sonnewald U. Neuronal and astrocytic shuttle mechanisms for cytosolic-mitochondrial transfer of reducing equivalents: Current evidence and pharmacological tools. Biochem Pharmacol. 2006; 71:399–407. [PubMed: 16368075]

Miller BL. A review of chemical issues in 1H NMR spectroscopy: N-acetyl-L-aspartate, creatine and choline. NMR Biomed. 1991; 4:47–52. [PubMed: 1650241]

Morrison BM, Lee Y, Rothstein JD. Oligodendroglia: metabolic supporters of axons. Trends Cell Biol. 2013; 23:644–651. [PubMed: 23988427]

Nicholson RM, Kusne Y, Nowak LA, LaFerla FM, Reiman EM, Valla J. Regional cerebral glucose uptake in the 3×TG model of Alzheimer's disease highlights common regional vulnerability across AD mouse models. Brain Res. 2010; 1347:179–185. [PubMed: 20677372]

Nunomura A, Castellani RJ, Zhu X, Moreira PI, Perry G, Smith MA. Involvement of oxidative stress in Alzheimer disease. J Neuropathol Exp Neurol. 2006; 65:631–641. [PubMed: 16825950]

Oakley H, Cole SL, Logan S, Maus E, Shao P, Craft J, Guillozet-Bongaarts A, Ohno M, Disterhoft J, Van Eldik L, Berry R, Vassar R. Intraneuronal beta-amyloid aggregates, neurodegeneration, and neuron loss in transgenic mice with five familial Alzheimer's disease mutations: potential factors in amyloid plaque formation. J Neurosci. 2006; 26:10129–10140. [PubMed: 17021169]

Perry EK, Perry RH, Tomlinson BE, Blessed G, Gibson PH. Coenzyme A-acetylating enzymes in Alzheimer's disease: possible cholinergic ‘compartment’ of pyruvate dehydrogenase. Neurosci Lett. 1980; 15:105–110. [PubMed: 6133246]

Pfeiffer SE, Warrington AE, Bansal R. The oligodendrocyte and its many cellular processes. Trends Cell Biol. 1993; 3:191–197. [PubMed: 14731493]

Ramos M, Pardo B, Llorente-Folch I, Saheki T, Del Arco A, Satrústegui J. Deficiency of the mitochondrial transporter of aspartate/glutamate aralar/AGC1 causes hypomyelination and neuronal defects unrelated to myelin deficits in mouse brain. J Neurosci Res. 2011; 89:2008–2017. [PubMed: 21608011]

Signoretti S, Marmarou A, Tavazzi B, Lazzarino G, Beaumont A, Vagnozzi R. N-Acetylaspartate reduction as a measure of injury severity and mitochondrial dysfunction following diffuse traumatic brain injury. J Neurotrauma. 2001; 18:977–991. [PubMed: 11686498]

Saab AS, Tzvetanova ID, Nave KA. The role of myelin and oligodendrocytes in axonal energy metabolism. Curr Opin Neurobiol. 2013; 23:1065–1072. [PubMed: 24094633]

Traka M, Wollmann RL, Cerda SR, Dugas J, Barres BA, Popko B. Nur7 is a nonsense mutation in the mouse aspartoacylase gene that causes spongy degeneration of the CNS. J Neurosci. 2008; 28:11537–11549. [PubMed: 18987190]

Vagnozzi R, Signoretti S, Tavazzi B, Cimatti M, Amorini AM, Donzelli S, Delfini R, Lazzarino G. Hypothesis of the postconcussive vulnerable brain: experimental evidence of its metabolic occurrence. Neurosurgery. 2005; 57:164–171. [PubMed: 15987552]

Vielhaber S, Kudin AP, Kudina TA, Stiller D, Scheich H, Schoenfeld A, Feistner H, Heinze HJ, Elger CE, Kunz WS. Hippocampal N-acetyl aspartate levels do not mirror neuronal cell densities in creatine-supplemented epileptic rats. Eur J Neurosci. 2003; 18:2292–2300. [PubMed: 14622190]

Wiame E, Tyteca D, Pierrot N, Collard F, Amyere M, Noel G, Desmedt J, Nassogne MC, Vikkula M, Octave JN, Vincent MF, Courtoy PJ, Boltshauser E, van Schaftingen E. Molecular identification

of aspartate N-acetyltransferase and its mutation in hypoacetylaspartia. Biochem J. 2009; 425:127–136. [PubMed: 19807691]

Highlights

- We analyze the expression of the NAA synthase gene, *Nat8L* in the 5xFAD mouse
- Downregulation of *Nat8L* is preceded by decreased energetic integrity
- Upregulation of catabolic ASPA also precedes decreased *Nat8L*
- *Nat8L* is dysregulated in ASPA-null mice, suggesting neuronal-glial crosstalk
- Pathological NAA reduction is a coordinated means of preserving energy substrate

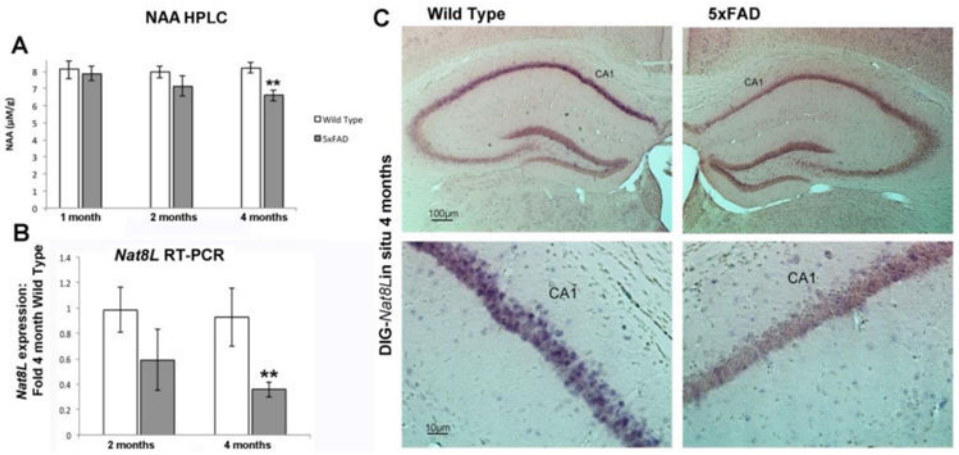

Figure 1.

Whole brain homogenates analyzed by HPLC show a significant reduction in NAA from 2-4 months of age in 5xFAD brains (**1A**; mean +/- SEM shown for each genotype at each age, n=7). QRT-PCR analysis of *Nat8L* expression 2-4 months of age showing a significant reduction in *Nat8L* at 4 months in 5xFAD brains (**1B**; expression presented as fold-4 month wild type, mean +/- SEM shown, n=5). *Nat8L* mRNA assessed by *in situ* hybridization at 4-months in wild type and 5xFAD brains showing prominent reductions in cells within the hippocampal CA1 subfield (**1C**).

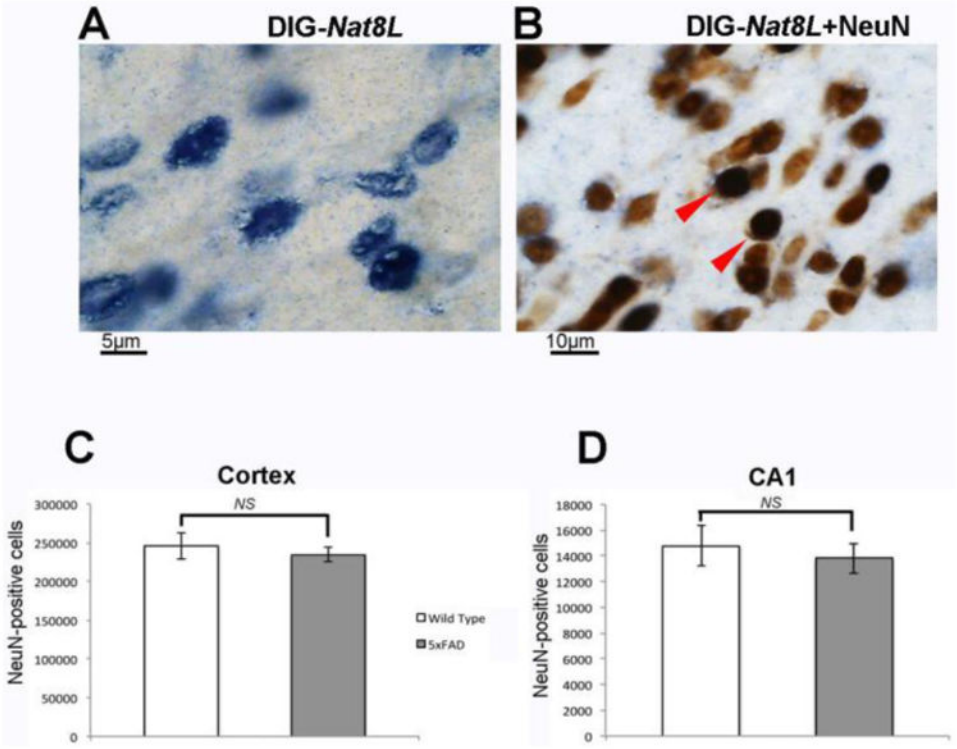

Figure 2.

(**2A**) Individual cells positive for *Nat8L* mRNA (blue nuclei), assessed using a DIG-labelled RNA probe (DIG-*Nat8L*). (**2B**) DIG-*Nat8L*-positive cells (blue) co-label with the neuronal nuclear antigen NeuN (brown) indicating neuronal expression. Stereological estimates of NeuN-positive cells in cortical layer V (**2C**) and CA1 of the hippocampus (**2D**) indicate no significant difference in neuron content in 4-month 5xFAD brains relative to wild type (mean +/- SEM, n=4).

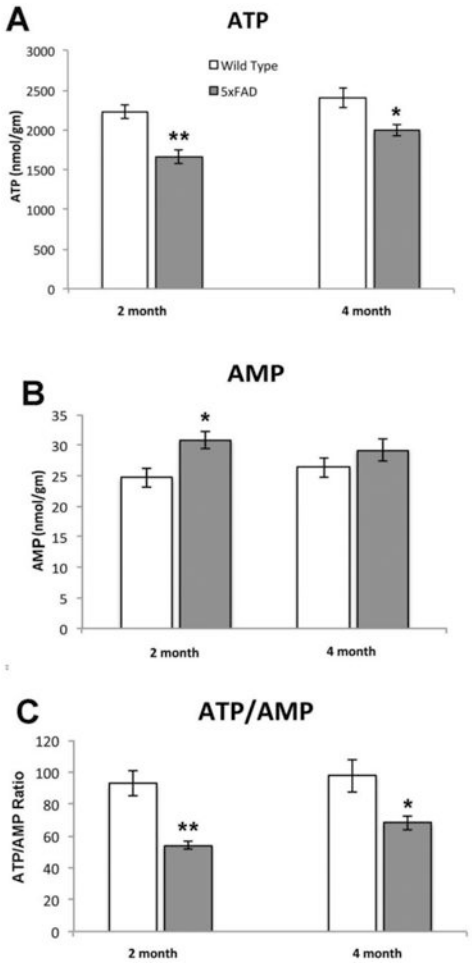

Figure 3.

HPLC analysis of ATP (**3A**) and AMP (**3B**) reveal significant decreases in the former and significant increases in the latter at 4-months in 5xFAD brains, resulting in a reduction in the ATP/AMP ratio (**3C**). Levels of ATP and AMP expressed as nmol/wet weight of tissue (mean +/- SEM shown for each group, n=7).

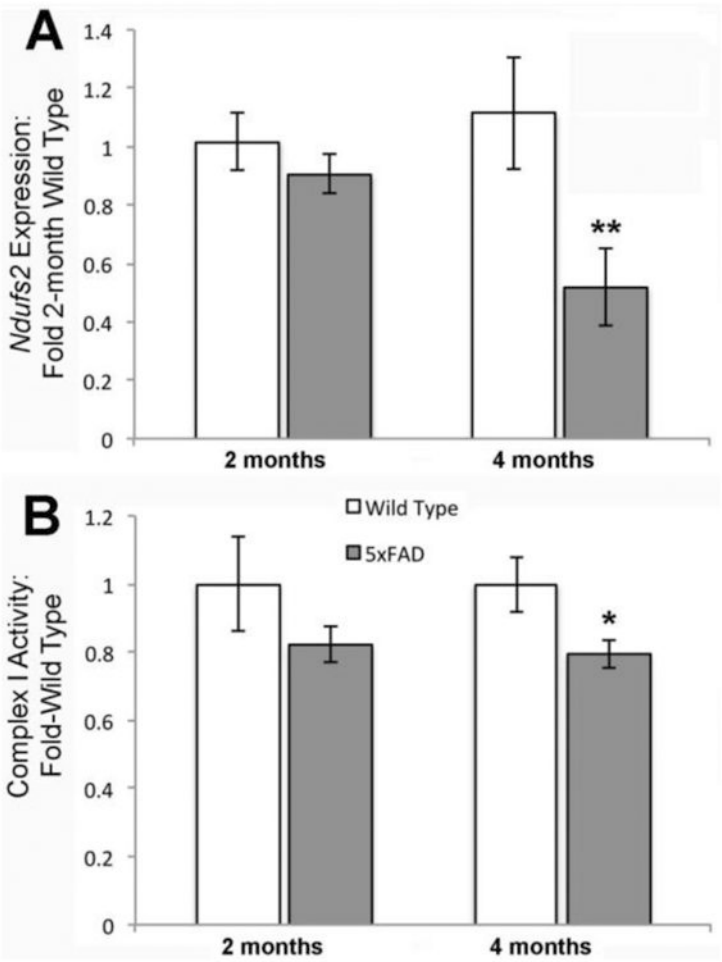

Figure 4.

(**A**) In-house QRT-PCR confirmation of the most significantly downregulated Complex I gene, *Ndusf2*, confirms 4-month array data (5xFAD values expressed as fold-2 month wild type values, +/- SEM, n=5. ******p≤0.01). Reduced *Ndusf2* expression correlates with a significant decrease in 4-month 5xFAD mitochondrial Complex I activity (**B; ***p≤0.05). Activity defined as the mean change in OD@450nm over 30 minutes. Values presented as fold-wild type activity, mean +/- SEM, n=5).

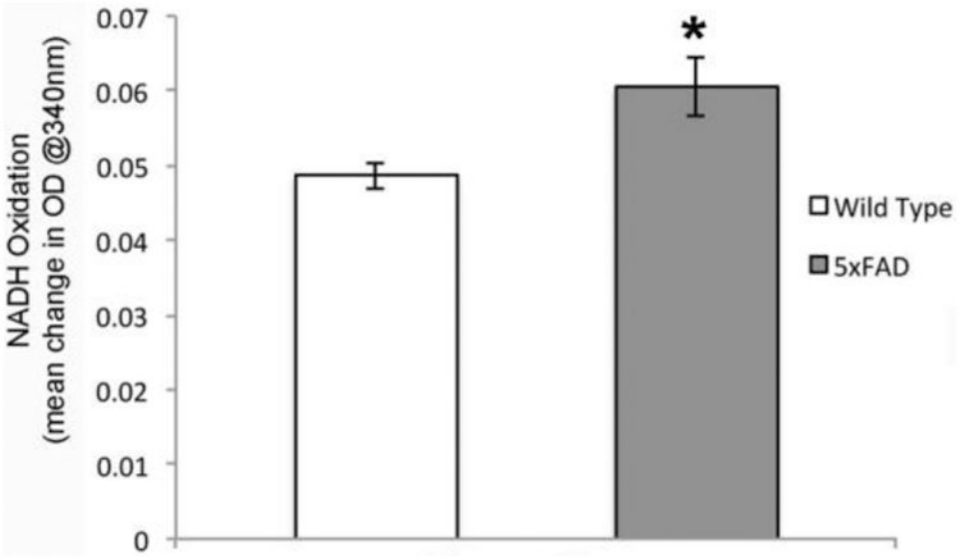

Figure 5.

Increased malate-aspartate shuttle (MAS) activity in 4-month 5xFAD brains relative to wild type controls. NADH oxidation, determined by the mean change in optical density (OD) @ 340nm over 5 minutes for 4-month 5xFAD and wild type mitochondrial preparations. Data expressed as mean change in OD +/- SEM, n=5. **p≤0.05.

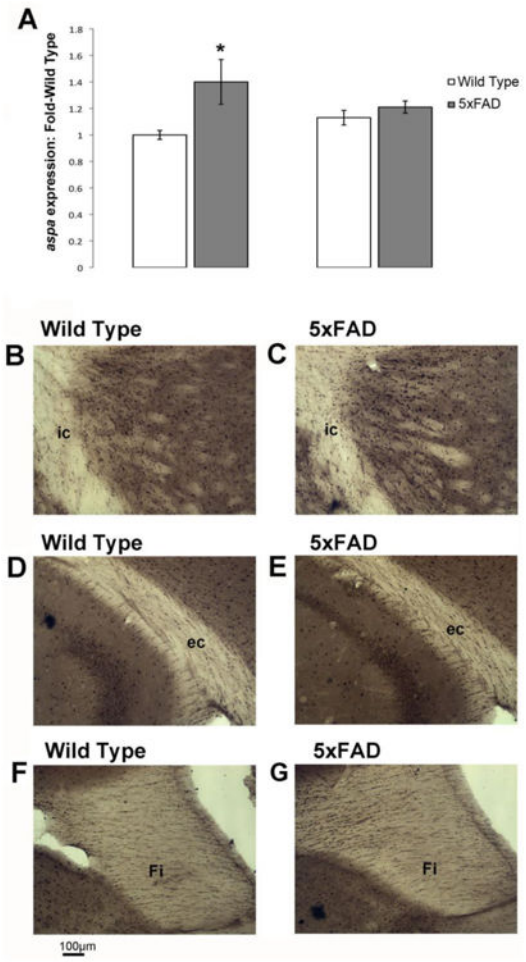

Figure 6.

(**A**) Increased *aspa* expression in 5xFAD brains at 2 months of age relative to wild type as assessed by QRT-PCR. *Aspa* expression presented as fold-wild type 2 month levels for each group, mean +/- SEM, n=5. Immunhistochemical evidence of increases in ASPA protein in 4-month 5xFAD brains within white matter tracts of the internal capsule (ic) adjacent to the thalamus (**B&C**), the external capsule (ec) overlying the hippocampus (**D&E**) and the white matter of the fimbria (Fi) of the fornix (**F&G**).

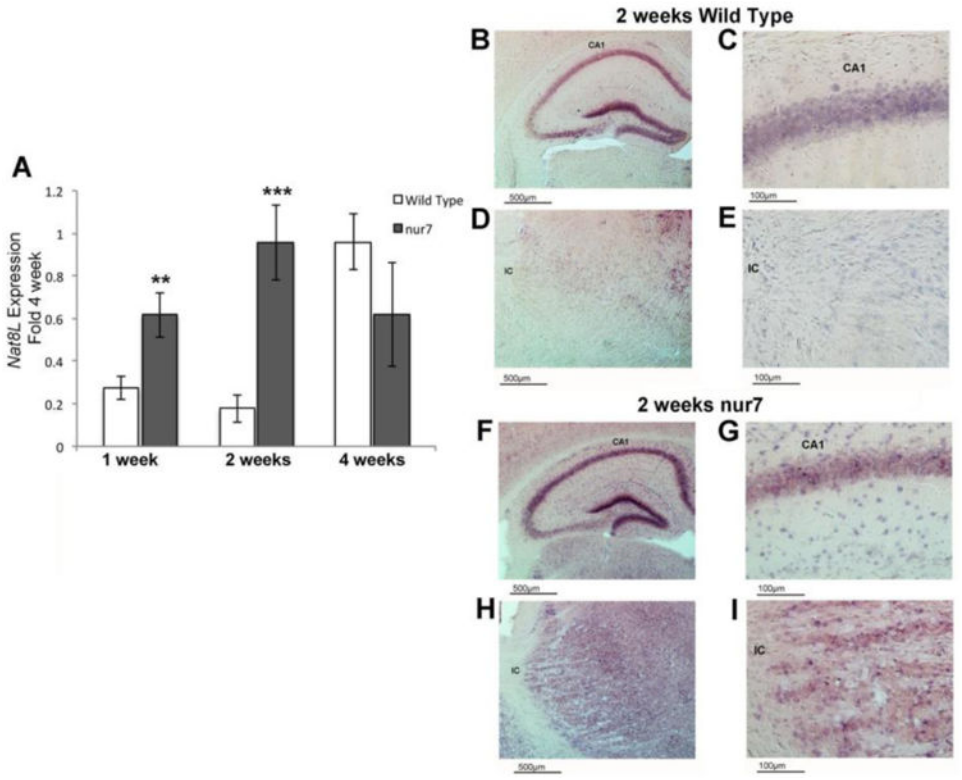

Figure 7.

Premature increases in *Nat8L* expression in theASPA-null *nur7* mouse brain at 2 weeks of age (**7A**; n=5), with *in situ* hybridization using a DIG-labeled *Nat8L* RNA probe showing clear increases in interneurons of the hippocampus (**7B-C & F-G**) and the thalamus (**7D-E & H-I**) on 2-month 5xFAD brains.

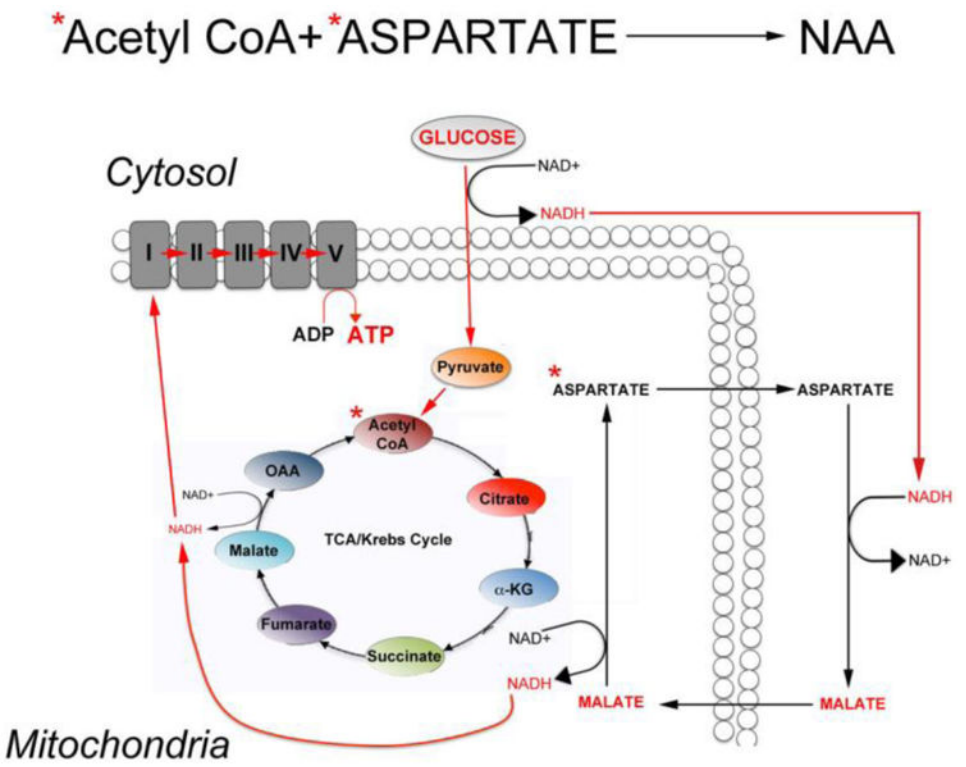

Figure 8.

Schematic showing the movement of carbon (red script) from glucose to ATP via the TCA/Krebs cycle and malate aspartate shuttle in neurons, highlighting the energetic cost of NAA synthesis by way of competing substrate. Glycolysis in the cytosol generates NADH, which is transported into mitochondria by the transamination of aspartate to malate to contribute substrate for oxidative phosphorylation by electron transport chain complexes I-V to yield ATP via the malate-aspartate shuttle. Oxidation of glucose to pyruvate generates Acetyl Coenzyme A (AcCoA), which drives the TCA cycle to generate intramitochondrial NADH for use by Complexes I-V of the electron transport chain, also yielding ATP. NAA synthesis requires both AcCoA and Aspartate (red asterisk), and competes for substrate, thereby defining NAA synthesis as energy-intensive and providing a rationale for the active downregulation of NAA synthesis in the face of pathology-induced energy crisis.

Table 1

Significant decreases in 13 nuclear-encoded genes for components of the mitochondrial electron transport chain, with a threshold significance of p=0.005, in 4-month 5xFAD brains as analyzed by microarray (n=3/genotype).

Gene	Complex	Fold-Wild Type
Ndufs2	I	-1.71
Uqcrh	III	-1.71
Bcs1l	III	-1.67
Atp5g3	V	-1.59
Cox5a	IV	-1.59
Ndufb3	I	-1.51
Atp5h	V	-1.46
Ndufa2	I	-1.44
Cox8c	IV	-1.44
Ndufs7	I	-1.41
Uqcrfs1	III	-1.41
Atp5j2	V	-1.39
Ndufb6	I	-1.37